FERMILAB-CONF-06-218-T

Measuring Velocities Using the CMB & LSS

Albert Stebbins[1,2]

[1] *Fermilab Particle Astrophysics Center, Box 500, Batavia, IL 60510, USA*
[2] *Institut d'Astrophysique de Paris, 98 bis Blvd Arago, 75014 Paris, FRANCE*
E-mail: stebbins@fnal.gov

Abstract

Here is discussed various ways by which the cosmic microwave background (CMB) radiation can be use to measure the velocities of matter in the universe. We include some new statistical techniques for using the kinetic Sunyaev-Zel'dovich (kSZ) effect and integrated Sachs-Wolfe (ISW) effect to determine velocities by correlating wide area CMB maps with overlapping large-scale structure (LSS) surveys.

Key words: cosmology: theory, cosmic microwave background, large-scale structure of the universe
PACS: 98.62.Py, 98.65.Cw, 98.65.Dx, 98.70.Vc

1 Why Measure Velocities

Much of cosmological observations involve the measurement of the (relative) positions of things: *e.g.* the clustering of galaxies, the angular structure of the CMB temperature and polarization anisotropies. It also interesting to concentrate on the measurements of the motion of things, *i.e.* (relative) velocities. The reasons for this are many:

- **Because they are there:** Often velocity information is encoded in measurements one makes for position information (*e.g.* redshift space distortions) so one gets velocities nearly for free.
- **Self Consistency**: The observed position of matter in the universe is obtained by the motion of the matter from it's (presumed) uniformly distributed initial condition. By comparing velocities and positions we can see if we get a self consistent picture for the formation of structure in the universe.
- **Forces**: The motion of matter in the universe is generated by forces acting upon the matter. By measuring velocities we can check if we understand the

forces which cause the formation of structure. The forces are mostly gravitational and this provides another test of gravity on cosmological length- and time-scales.

2 Traditional Approaches to Velocity Using the CMB

Many of the major contributions to CMB anisotropies are fairly direct measurements of velocities (combined with other quantities). One has always expected velocity information from the CMB, so much so that the peak structure of the CMB angular power spectrum was, in the past and somewhat misleadingly, often called the "Doppler peaks".

2.1 The Integrated Sachs-Wolfe (ISW) Effect

An important contribution to the standard model of anisotropies is the integrated Sachs-Wolfe (ISW) effect (20). This is usually written in terms of a line-of-sight integral of the time varying gravitational potential

$$\frac{\Delta T_{\rm ISW}}{T} = \frac{2}{c^3}\int dl\, e^{-\tau}\dot{\Phi}\,, \tag{1}$$

where dl is the path length, τ the Thompson optical depth (see below), and Φ the peculiar gravitational potential (*i.e.* deviation of the potential from it's value in a homogeneous cosmology). Of course, the reason for the time-varying potential is that matter is moving around, *i.e.* because of velocities. This is evident from the expression [1]

$$\frac{1}{4\pi G}\nabla^2\dot{\Phi} = \frac{\partial\left(a^2(\rho_{\rm m}-\overline{\rho_{\rm m}})\right)}{\partial t} = -a^2 H(\rho_{\rm m}-\overline{\rho_{\rm m}}) - a\,\nabla\cdot(\rho_{\rm m}\mathbf{v}) \tag{2}$$

where a is the cosmic scale factor, ∇ the comoving gradient, $\rho_{\rm m}$ the matter density, $\overline{\rho_{\rm m}}$ it's mean, $\mathbf{v}$ the peculiar velocity (*i.e.* wrt the cosmic rest frame), and H the Hubble parameter. Note that even the first term, $\propto H$, can be interpreted in terms of velocities since H is the mean cosmological velocity gradient. Thus we can say that the ISW anisotropies are caused by velocities.

For small growing mode inhomogeneities $\nabla\cdot\mathbf{v} = -a\,H\,f\,\delta_{\rm m}$ where $\delta_{\rm m} = \frac{\rho_{\rm m}}{\overline{\rho_{\rm m}}} - 1$, $f = \frac{d\ln[g]}{d\ln[a]}$, $g[a]$ is the linear growth function, and $\Omega_{\rm m} = \frac{8\pi G\overline{\rho_{\rm m}}}{3H^2}$. Using

[1] This is an expression for non-relativistic matter but may include a Λ.

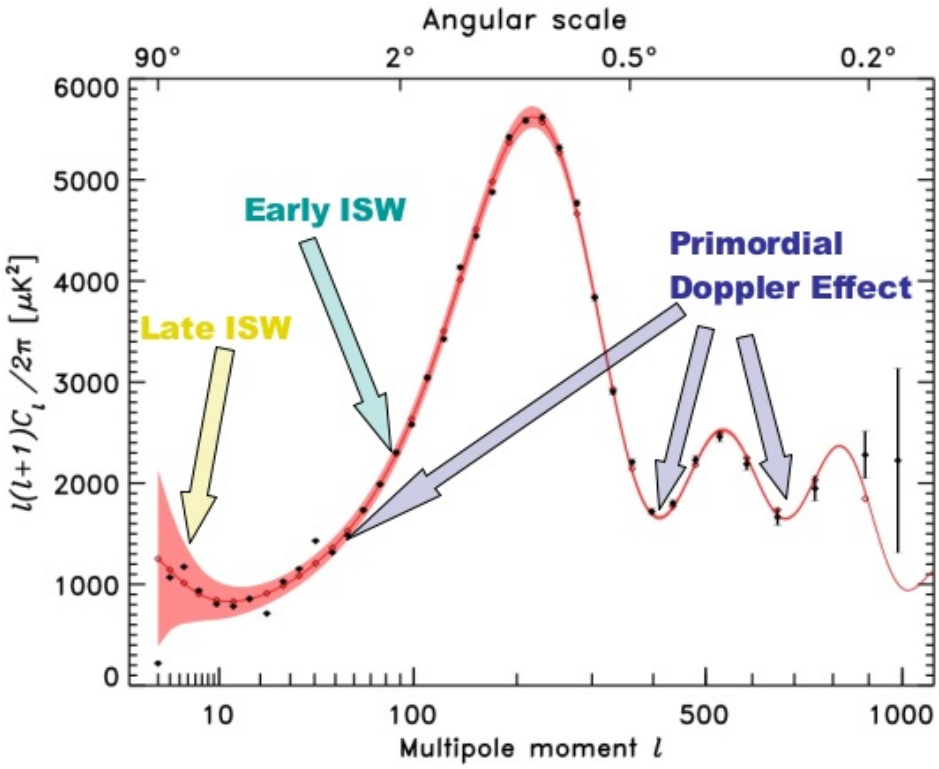

Fig. 1. Taken from Hinshaw *et al.* 2006 with annotations. The dots represent the WMAP 3 year data anisotropy angular power spectrum while the shaded band the best fit ΛCDM predictions with sample variance. While most of the power is from the Sachs-Wolfe effect on large scale, and adiabatic heating on small scales, the arrows indicate regions most sensitive the early- and late-time ISW effect as well as the primordial Doppler effect. We argue in the text that these effects are fairly direct indicators of velocity flows of the dark matter and gas. The fact that the model fits so well is indicative that the velocities are just as expected.

$dl = c\,dln[a]/H$ the ISW integral becomes

$$\frac{\Delta T_{\rm ISW,linear}}{T} = -3 \int d\ln[a]\, e^{-\tau} \Omega_{\rm m}\, (1-f)\, \left(\frac{c\,\nabla}{a\,H}\right)^{-2} \delta_{\rm m}\,. \tag{3}$$

The factor $1 - f \propto a\,H - \nabla \cdot \mathbf{v}/\delta_{\rm m}$ is a weighted difference of cosmic velocity gradients (H) and peculiar velocity gradients ($\nabla \cdot \mathbf{v}$). For pressureless growth $f \approx {\Omega_{\rm m}}^{0.6}$ so the two cancel when $\Omega_{\rm m} = 1$ in which case the ISW effect is zero. In the now standard flat ΛCDM model $\Omega_{\rm m}$ deviates significantly from unity at $z \lesssim 1$ and $z \gtrsim 10^3$. Also before recombination ($z \approx 1100$) pressure forces become important for growth. So at both early times and late times we expect a significant ISW contributions to the CMB anisotropy.

2.1.1 ISW from CMB Alone

The standard ΛCDM model gives an extremely accurate description of the CMB anisotropy data, as is best illustrated in the 3-year WMAP data (see Fig. 1) (12; 24). The early-time ISW must be as predicted at $l \sim 100$ for such a good fit. There is also a significant indication of the late-time ISW contribution at $l \sim 4$. The good model fit suggests that the velocity gradients are near to their expected values both at $z \sim 10^3$ and $z \lesssim 1$, and in this sense we can say we have velocity determinations.

2.1.2 ISW in Cross-Correlation

The late-time ISW contributions to the anisotropies become very small for $l > 7$, so much so that we expect no distinctive evidence for the ISW effect at intermediate l's using the CMB alone. However much of the expected ISW contribution comes from velocities generated by the gravitational attraction of matter associated with objects we can see; in particular QSO's and galaxies which can be observed via optical and radio large scale structure (LSS) surveys. By correlating the angular pattern of clustering of these objects with the CMB temperature pattern we can extract the ISW contribution on these intermediate scales. Large areas of the sky must be covered and even with the ultimate survey the ISW detected through this cross-correlation method is expected to have a significance of $< 10\sigma$ (7). Nevertheless several groups have detected this cross correlation using WMAP data (4; 8; 23; 9; 18; 31). The significance of the combined detection is at $\sim 5\sigma$. [2]

2.2 The Kinetic (or Kinematic) Sunyaev-Zel'dovich (kSZ) Effect

The kinetic Sunyaev-Zel'dovich effect (kSZ) has long been known to give an important contribution to the CMB temperature anisotropies (27). The kSZ (or "Doppler") anisotropy is described by an integral along the line-of-sight

$$\frac{\Delta T_{\rm kSZ}}{T} = \frac{v_\parallel^{\rm eff}}{c} \qquad\qquad v_\parallel^{\rm eff} \equiv \int d\tau\, e^{-\tau}\, v_\parallel\,, \tag{4}$$

where $v_\parallel$ is the component of the gas velocity in the CMB frame in the direction of the observer, $d\tau = \sigma_{\rm T}\, n_{\rm e}\, dl$ is the Thomson optical depth, dl is the path length, $n_{\rm e}$ is the density of free electrons, and $\sigma_{\rm T}$ the Thomson cross-section.

[2] R. Scranton private communication.

2.2.1 kSZ: The Primary Doppler Effect

At the surface of last scattering where τ becomes large, $\int d\tau\, e^{-\tau} \to 1$, so $v_{\parallel}^{\rm eff}$ can be interpreted as an average velocity, *i.e.* $v_{\parallel}^{\rm eff} \to \overline{v_{\parallel}}$, and we obtain the usual expression for a non-relativistic Doppler-shifted emission: $\frac{\Delta T}{T} = \frac{\Delta\nu}{\nu} = \frac{v_{\parallel}}{c}$ (15).

At the surface of last scattering kSZ/Doppler contributes about a third of the small scale primordial anisotropies (14). As with the early-time ISW we can argue that since the standard model of anisotropies produces such a good fit to the observed anisotropies that we should believe that the Doppler terms are as expected at the surface-of-last-scattering, and in this sense the corresponding velocities have been detected.

2.2.2 kSZ: Clusters

As with the early efforts of detecting the thermal Sunyaev-Zel'dovich (tSZ) effect most of the observational effort on detecting the kSZ in the low redshift universe have concentrated on looking at clusters where the signal is relatively large. Note however that unlike tSZ, kSZ is not weighted toward hot gas, and since all objects, big/hot and small/cold, will be moving with the cosmological flow, the largest $\Delta T_{\rm kSZ}$ comes from the objects with largest τ, which are galaxies not clusters of galaxies. However galaxies are too small and not well matched to most CMB experiments. Furthermore the central regions of galaxies are sites of much radio, mm, and sub-mm emission, which will complicate any kSZ measurement. So clusters are probably the easiest places to look for a kSZ signal. Clusters are also the site of a tSZ signal much larger than the kSZ signal. To subtract off the tSZ one needs mm-wave observations which are particularly difficult from the ground. Only upper limits on cluster peculiar velocities have been set so far (13) although we can expect detections in the near future by SPT, ACT, and the Planck Surveyor (2; 16; 19; 11).

3 New Approaches to Velocity Using the CMB

Both CMB and LSS data are getting much better and we can use these bigger better datasets to get more velocity information out of the CMB. In what follows we propose to do what was done with the intermediate scale ISW (Sec. 2.1.2): namely to correlate CMB observations with overlapping LSS surveys. The LSS tells us where the mass is and thus the pattern of velocities. By measuring the correlations we are effectively weighing the mass correlated with the LSS. There is, no doubt, some mass uncorrelated with objects we observe, and one we will not find this mass or the associated velocities with

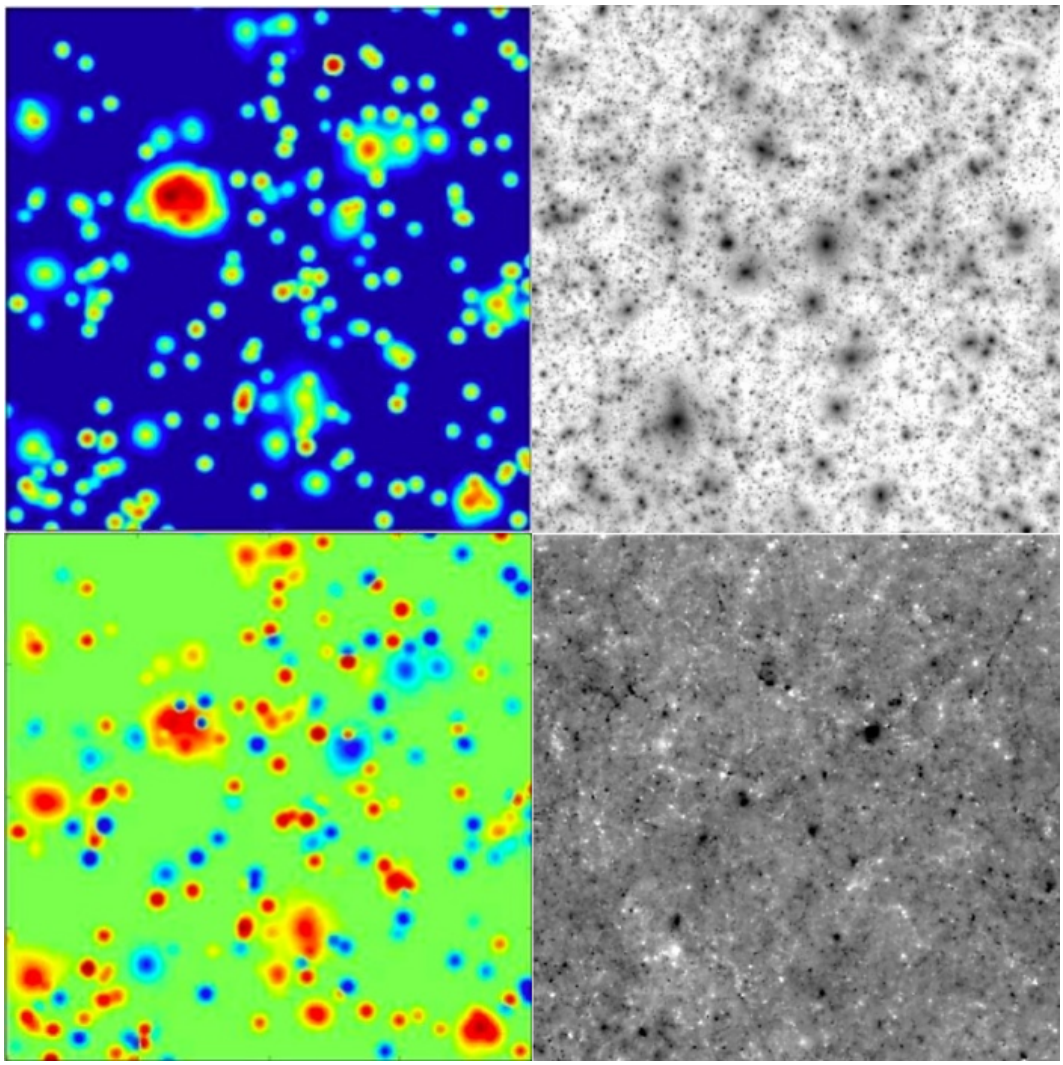

Fig. 2. Shown are four simulated CMB anisotropy maps. The top row includes only the tSZ effect while the bottom row includes only the kSZ effect, which has both positive and negative anisotropies. The left column is taken from Schäfer *et al.* 2004 whose simulations included only the contribution from galaxy clusters, while the right column is taken from Springel *et al.* 2001 whose simulations include all of the gas. The scales for the two columns are different and the reader should refer to the original papers for all details. The point being made here is the qualitative similarity of the top left and right maps, meaning that a superposition clusters gives a good description of the tSZ emission as a whole. This is in contrast to the qualitative dissimilarity of the bottom two maps, meaning that the cluster kSZ contribution, on the bottom left side, does not give a qualitatively adequate description of the entire kSZ pattern on the bottom right side, which has much more structure in it. That is to say, the cluster kSZ signal is only a fraction of the total kSZ signal. There is much more to kSZ than just clusters or virialized objects!

these techniques. We do not expect much uncorrelated mass.

The LSS also gives us additional information for the kSZ effect: namely a good

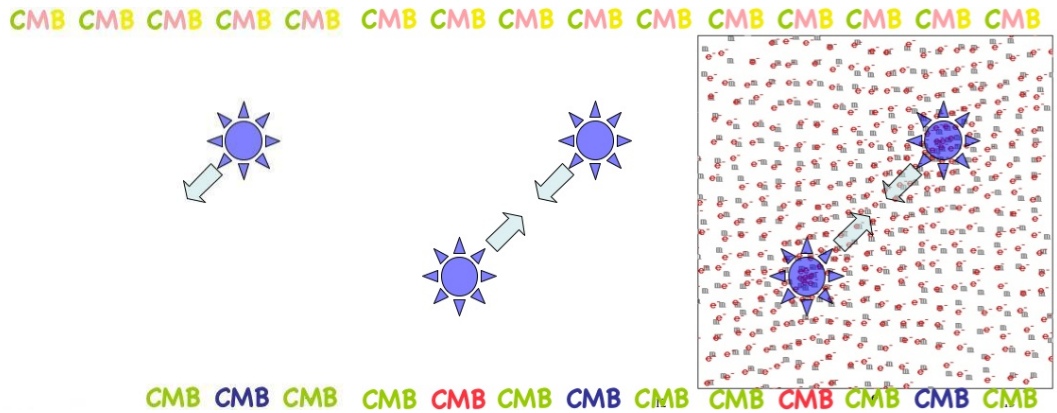

Fig. 3. Three cartoons illustrating different approaches to measuring the kSZ effect. In all figures the surface-of-last-scattering is at the top is and on the observer the bottom. The starred object is a cluster of galaxies and the arrow represents it's motion. The left figure represents the usual sort of measurement: one looks at a single cluster and we look for a CMB hotspot or coldspot. On the middle there are two clusters, which, on average, will be moving toward each other since clusters are correlated with mass which attracts other clusters. If we determined that the one was more distant than the other we would expect, on average, the one behind to produce a hotspot and the one in front to produce a cold spot. This is in contrast to other sorts of emission from the two clusters (*e.g.* tSZ), for which we expect the same sign ΔT. Using multiple clusters one can use expected velocity correlations, which depends on the observed 3-d spatial distribution of the clusters to increase the S/N of a kSZ measurement. On the right we have added m's representing mass (mostly dark matter) and e^-'s representing free electrons. The overdensity in m's and e^-'s is not localized in the cluster but extends well beyond the cluster. This illustrates the idea that the mass correlated with an observed cluster is much larger than the mass contained within the cluster. So one shouldn't use the cluster mass to estimate the infall velocity of other clusters toward a given cluster but the much larger correlated mass. It also illustrates the idea the number of electrons associated with a cluster which partake in a common flow is much greater than the electrons within the cluster itself. One shouldn't necessarily match the CMB beam to the size of the cluster.

indication of where the free electrons are, *i.e.* $n_{\rm e}$ in Eq. 4. This is especially significant for kSZ which is proportional to the line-of-sight component of $\mathbf{v}$, Since $\nabla \times \mathbf{v} \approx 0$, the line-of-sight velocity tends to integrate out to small values unless modulated by a fluctuating $n_{\rm e}$ (17). The LSS tells us where these fluctuations are and provide a good template for the kSZ signal. The use of LSS objects as tracers for mass and electrons is illustrated in Fig. 3, which emphasizes that we can use all of the mass and electrons correlated with the LSS objects and not the much smaller mass and number of electrons contained within the objects themselves.

CMB velocity estimators (ISW or kSZ) are always contaminated by other sources of emission *e.g.* primary CMB or radio emission. Traditional methods of dealing with these are

- **1** Use multi-band CMB measurements to spectrally discriminate the signal from the contamination *e.g.* tSZ, synchrotron emission, *etc.* This cannot remove primary CMB which has the same spectra as ISW and kSZ.
- **2** Apply angular pattern filters to remove the contamination. This includes masking bright sources (*e.g.* point sources or strong tSZ emission) or adjusting a synthetic beam to maximize signal (kSZ, ISW) to noise (primary CMB or lensed CMB, *etc.*). (10)
- **3** Use large statistical samples, *e.g.* for cluster kSZ. Even if for individual clusters the kSZ S/N was small, if one could show that the rms value of a velocity estimator applied to a cluster was larger than that applied to a random field, one could argue you had detected velocities. Of course, the problem would be that there are many other reasons why a CMB signal would be larger when in the direction of a cluster.

Other sorts of spatial filtering can also be applied when cross-correlating velocity estimators in different directions:

- **4** The velocity field is correlated over large distances. By looking only at cross-correlations of velocity estimators in different directions, not auto-correlations in the same direction, one can statistically remove localized contamination of the signal *e.g.* tSZ or radio emission. (11; 32)
- **5** The velocity field does fall off at sufficiently large distances, but other sorts of contamination are not localized but rather have no particular dependence on separation. By subtracting off the covariance at large separation (which also subtracts the mean), *e.g.* $\langle \mathbf{v}_1 \mathbf{v}_2 \rangle [\vartheta] - \langle \mathbf{v}_1 \mathbf{v}_2 \rangle [\infty]$, one can statistically remove such contamination.

LSS information allows one to add additional techniques to this list

- **6** Even where one has good CMB coverage, for $z \lesssim 1$ one can typically find many more clusters using multi-color optical photometry than from their SZ decrement. This allows better identification of high signal regions and better statistics. With LSS one can use low resolution CMB data which cannot find many clusters; or use the LSS to find larger scale non-virialized concentrations of gas and mass.
- **7** Spectroscopy or multi-color photometry will give accurate estimates of the redshift of LSS, something the CMB cannot do at all. This allows better selection of nearby correlated velocities in 3-d, and thus less dilution of the signal. (32)
- **8** The 3-d spatial pattern of LSS gives a template for the expected velocity pattern. The velocity signal will correlate with this template, while usually the contaminants will not. One reason for this lack of correlation is usually that the velocity is a vector quantity while the contaminants are scalar quantities. The LSS also supplies a template for the mass which enters the non-linear ISW and for the electron overdensity which enters the non-

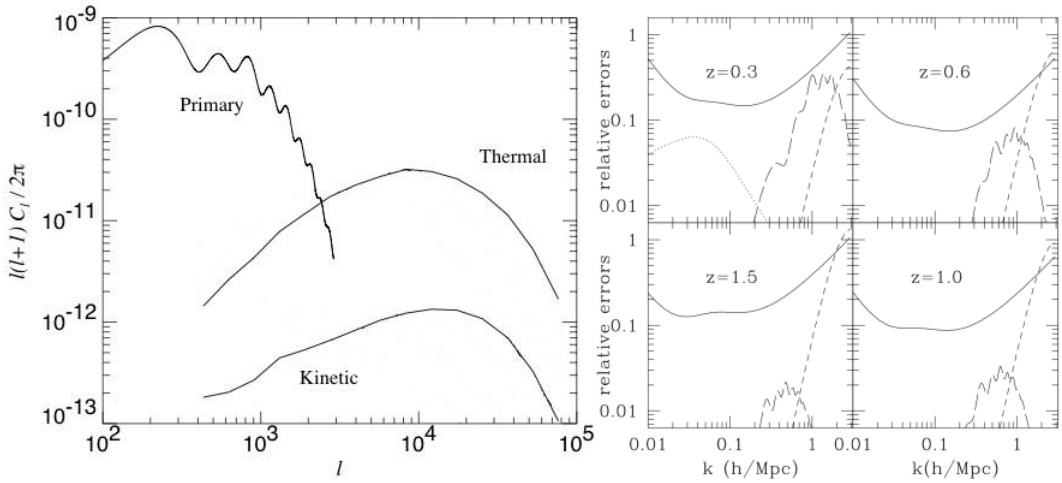

Fig. 4. The left figure taken from Springel *et al.* (2001). This is an estimate of the angular power spectrum of $\frac{\Delta T}{T}$ broken up into contributions from from primary (linear), tSZ, and non-linear kSZ effects. The right figure is taken from Zhang *et al.* (2004) and gives the fractional statistical error in estimates of the cluster-cluster kSZ cross power spectrum, in 3-d k-space with bins $\Delta k = 0.4 \sim k$, $\Delta z = 0.2$, and sky coverage $f_{\rm sky} \sim 0.1$. The lower lines give contamination from correlated sources (dotted), Cosmic Infrared Background + other kSZ (short dashed), and primary CMB (long dashed). The error is dominated by an assumed $35\,\mu$K rms shot noise per cluster, which includes instrumental noise and unsubtracted tSZ. The left plot is discouraging, the right encouraging.

linear kSZ. The template technique allows one to look for a velocity-LSS correlations, not only velocity-velocity correlations. In terms of S/N one typically finds that $\frac{{\rm Var}[\langle \hat{v}\,\hat{\delta}\rangle]}{\langle v\,\delta\rangle^2} \sim \frac{{\rm Var}[\hat{v}]\,{\rm Var}[\hat{\delta}]}{\langle v\,\delta\rangle^2} \ll \frac{{\rm Var}[\langle \hat{v}\,\hat{v}\rangle]}{\langle v\,v\rangle^2} \sim \frac{{\rm Var}[\hat{v}]^2}{\langle v\,v\rangle^2}$, *i.e.* velocity estimators are noisier than density estimators, so velocity-LSS correlation estimators are less noisy than velocity-velocity correlation estimators.

Now let us consider some (theoretical) applications of these techniques.

3.1 kSZ: 3-d Velocity Correlations

As indicated in Fig. 4 the overall kSZ signal after recombination is very small compared to the primary CMB and tSZ anisotropies. However by concentrating on clusters, and using techniques 1-7 above, Zhang *et al.* (2003) has modeled the estimation of the cluster line-of-sight velocity-velocity correlation in 3-d. The estimator is, roughly, $\overline{T_a\,T_b}[\vartheta_{ab}] - \overline{T_a}^2$ where T_a and T_b are the suitably filtered CMB temperature in the direction of a clusters a and b, while ϑ_{ab} is their angular separation. As illustrated in Fig. 4 the S/N for this correlation estimator can be fairly good over a range of scales and a range of redshifts.

3.2 kSZ: Infall Velocity

As illustrated in Fig. 3 the observed LSS objects tend to attract one another. With distance information from LSS one can predict the sign of $v_\parallel$ and hence $\langle T_a \rangle_{\rm kSZ}$ using technique 8. One can construct an estimator

$$\hat{V}_{\rm infall}[\vartheta_{ab}] = \overline{{\rm sgn}[\hat{z}_a - \hat{z}_b]\, w[\hat{z}_a, \hat{z}_b]\, (T_a - T_b)}[\vartheta_{ab}] \tag{5}$$

where the $\hat{z}_a$ are the redshift (distance) estimators of LSS sources. So long as ${\rm sgn}\,[w[\hat{z}_a, \hat{z}_b; \vartheta_{ab}]] = {\rm sgn}\,[\hat{z}_a - \hat{z}_b]$ we would expect that $\langle \hat{V}_{\rm infall} \rangle_{\rm kSZ} > 0$.[3] Since $\langle T_{\rm primary} \rangle = 0$ to a good approximation $\langle \hat{V}_{\rm infall} \rangle_{\rm primary} = 0$.[4] For small $|z_a - z_b|$ most other contaminants are independent of ${\rm sgn}[z_a - z_b]$ and do not contribute to $\langle \hat{V}_{\rm infall} \rangle$. For larger $z_a - z_b$ the slow z evolution of $\langle T_a \rangle$ (non-kSZ signal correlated with LSS) can contribute, but can be removed by method 5, *i.e.* by using $\hat{V}_{\rm infall}[\vartheta] - \hat{V}_{\rm infall}[\infty]$. This method can use all of the techniques outlined above, and can be be applied not only to clusters of galaxies but to other LSS tracers such as galaxies.

3.3 Small Scale ISW: the Slingshot Effect

For the late-time ISW on the very smallest angular scales, where the overdensity is large and density gradients are larger than the velocity gradients, one finds that the leading order contribution to the ISW integral looks like

$$\frac{\Delta T_{\rm ISW,slingshot}}{T} \approx -2 \int d\ln[a]\, \mathbf{v}_\perp \cdot \left(\frac{\nabla}{a\, H} \right) \frac{\Phi}{c^2}\,, \tag{6}$$

where $\mathbf{v}_\perp$ is the the peculiar velocity transverse to the line-of-sight (the parallel gradients integrate out to give a smaller contribution). In practice this term is dominated by the transverse motion of the virialized objects with the deepest potential wells, *i.e.* clusters of galaxies (3; 26; 29; 30) producing a cold spot in front and a hot spot behind. This effect on the photons is analogous to the method used to boost deep space probes into the outer parts of the Solar System by sending them behind massive planets. This is called the slingshot effect and we use the same name. One might hope to use the hot/cold spot signature to extract it. Unfortunately kSZ and lensing of the primary anisotropies can produce similar patterns with greater frequency (1; 5) (see Fig. 3-right). However we can go further and use technique 8 to correlate the temperature

[3] For large separations infall velocity and mass can be anti-correlated and $\langle \hat{V}_{\rm infall} \rangle_{\rm kSZ} < 0$.

[4] There is a small correlation of LSS and $T_{\rm primary}$, *e.g.* ISW, which may enter.

gradient across the cluster with the LSS surrounding the cluster, and extract the slingshot signal. Neither the kSZ or the lensed CMB will contribute to these correlation. With very large number statistics one can hope to detect the slingshot effect. With a detection we can compare $\Delta T_{\rm slingshot}$ with cluster mass determinations from weak lensing, the ratio of the two is $\propto \beta \approx {\Omega_{\rm m}}^{0.6}/b$ where b is the bias of the LSS tracers we use.

3.4 Velocity Induced Polarization

The passage of (CMB) photons through a moving ionized medium will induce linear polarization (28). In tensor form it is $\propto \mathbf{v}_\perp \otimes \mathbf{v}_\perp - \frac{1}{2}\mathbf{I}\,|\mathbf{v}_\perp|^2$ where $\mathbf{v}_\perp$ is the transverse velocity in the CMB frame. This is because a Doppler shifted CMB has a quadrupole component. The velocity quadrupole is typically smaller than the Sachs-Wolfe quadrupole and the latter will mask the former (6). Using technique 8 one can determine the expected velocity-induced polarization orientation with LSS measurements, and since the spatial correlation length of velocities is much smaller than that of the Sachs-Wolfe quadrupole, one can hope to separate out the two. Even if one is mostly interested in the Sachs-Wolfe effect, one can use this technique to remove some of the velocity contamination.

4 Summary

Measurement of CMB anisotropies have long encoded information about velocities in the universe: the obvious Doppler / kSZ contribution, and the less obvious ISW contribution. New techniques for combining CMB measurement with LSS measurements to extract even more velocity information out of the CMB are outlined here. Most of these techniques have not yet been implemented. They require large statistical samples provided by large area overlapping CMB and LSS surveys. Many of these measurements will become available in the next few years.

Acknowledgements

This work was supported by the DOE and the NASA grant NAG 5-10842 at Fermilab. The author is grateful for the hospitality of the Institut d'Astrophysique de Paris where this manuscript was written.

References

[1] N. Aghanim, S. Prunet, O. Forni, & F.R. Bouchet, *A&A* **334** 409 (1998).
[2] N. Aghanim, K. Gorski, & J.-L. Puget, *A&A***374** 1 (2001).
[3] M. Birkinshaw & Gull, *Nature* **302** 315 (1983).
[4] S. Boughn & R. Crittenden, *Nature* **427** 45 (2004);
[5] A. Cooray, *Phys. Rev.* **D65** 083518 (2002).
[6] A. Cooray & D. Baumann, *Phys. Rev.* **D67** 063505 (2003).
[7] R. Crittenden & N. Turok, *Phys. Rev. Lett.* **76** 575 (1996).
[8] P. Fosalba & E. Gaztañaga, *MNRAS* **350** L37 (2004);
[9] P. Fosalba, E. Gaztañaga, & F. Castander *Ap. J.* **597** L89 (2003);
[10] M.G. Haehnelt & M. Tegmark, *MNRAS* **279** 545 (1996).
[11] C. Hernandez-M., L. Verde, R. Jimenez, & D.N. Spergel, *Ap. J.* **643** 598 (2006).
[12] G. Hinshaw, *et al.* [preprint arXiv: astro-ph/0603451];
[13] W.L. Holzapfel *et al.* **Ap. J. 481** 35 (1997).
[14] W. Hu & N. Sugiyama, *Ap. J.* **444** 489 (1995).
[15] N. Kaiser, *Ap. J.* **282** 374 (1984).
[16] A. Kosowsky, *New Ast. Rev.* **47** 939 (2003).
[17] J.P. Ostriker & E.T. Vishniac, *Ap. J.* **306** L51 (1986);
[18] N. Padmanabhan *et al.*, *Phys. Rev.* **D72** 043525 (2005);
[19] J.E. Ruhl *et al.* , *Proc. SPIE* **5498** 11 (2004).
[20] R.K. Sachs & A.M. Wolfe, *Ap. J.* **147**, 73 (1967).
[21] S. Y. Sazonov & R. A. Sunyaev, MNRAS **310**, 765 (1999).
[22] B.M. Schäfer, C. Pfrommer, M. Bartelmann, V. Springel, & L. Hernquist [preprint arXiv: astro-ph/0407089].
[23] R. Scranton *et al.* , [preprint arXiv: astro-ph/0307335];
[24] D. Spergel, *et al.* [preprint arXiv: astro-ph/0603449].
[25] V. Springel, M. White, & L. Hernquist, *Ap. J.* **549** 681 (2001).
[26] A. Stebbins, *Ap. J.* **327** 584 (1988).
[27] R.A. Sunyaev & Y.B. Zeldovich, *Ap. Sp. Sci.* **7** 3 (1970).
[28] R.A. Sunyaev & Y.B. Zel'dovich, MNRAS **190**, 413 (1980).
[29] R. Tuluie & P. Laguna, *Ap. J.* **445** L76 (1995).
[30] R. Tuluie, P. Laguna, & P. Aninos, *Ap. J.* **463** 15 (1996).
[31] P. Vielva, E. Martinez-G., & M. Tucci [preprint arXiv: astro-ph/0408252].
[32] P. Zhang, A. Stebbins, R. Juszkiewicz, & H. Feldman [preprint arXiv: astro-ph/0410637].